In-line digital holography for dynamic metrology of MEMS

Invited Paper

Vijay Raj Singh* **and Anand Asundi**

School of Mechanical and Aerospace Engineering, Nanyang Technological University, Singapore, 639798

**E-mail: vr.singh@pmail.ntu.edu.sg*

Received June 18, 2009

In-line digital holography helps to relax the spatial resolution requirement on charge-coupled device sensors for digital recording of holograms and to utilize the full sensing area for image reconstruction which provides larger field of view and better imaging resolution. In this letter, a lensless in-line digital holographic microscopy is presented for dynamic metrology of micro-electro-mechanical systems devices. The methodologies of interferometry and time-averaged in-line digital holography are presented for dynamic measurements, which are also useful for simultaneous suppression of in-line waves from real image wave. The experimental results are presented for dynamic thermal characterization of microheater and vibration analysis of cantilevers.

OCIS codes: 090.1995, 090.2880, 120.5050, 120.3180, 120.7280, 120.4290.

doi: 10.3788/COL20090712.1117.

Recent technological development and miniaturization of the test object features create new challenges for optical metrology, e.g., to provide convenient tool for whole field imaging and micro-systems characterization, and to provide experimental data for computer aided engineering for fast and accurate measurements, etc. The requirements are better measurement system performance for full three dimensions (3D), large field of view, and high imaging resolution, as well as real time analysis. Holography is an important tool for optical metrology[1]. In digital holography (DH), digital recording devices (e.g., charge-coupled device (CCD) sensor) provide flexibility to record holograms directly in digital form[2]. The reconstruction process is then performed numerically, giving quantitative analysis of amplitude and phase of the wavefront. This offers new possibilities for a variety of applications[3−5].

The integration of mechanical elements, electronics, sensors, and actuators on a common silicon substrate by micromachining technology constitutes micro-electro-mechanical systems (MEMSs)[6,7]. Characterization of the mechanical properties of MEMS structures at different stages of manufacturing is very significant. The purpose of dynamic MEMS testing is to provide feedback about device behaviour, system parameters, and material properties for design and simulation process. Also dynamic testing is needed in final devices to test their performance, characteristics, and reliability. Dynamic characterization of the mechanical properties of MEMS structures is a challenging task.

The capability of whole field information storage in holography method and the use of computer technology for fast data processing open the new possibilities to develop DH as a dynamic metrological tool for MEMS and micro-systems[8]. As a noble method, DH has received increased attention and has been developed for various applications of micro-systems measurement in the last few years[9−11]. The most current methodologies of DH are mainly based on off-axis system geometry which utilizes only partial area of CCD sensor and provides poor imaging resolution during reconstruction[12]. In contrast, the in-line system helps to relax the spatial resolution requirement on CCD sensors and to utilize the full sensing area which provides larger field of view and better imaging resolution[13]. The main limitation of in-line based geometry of DH system is the overlapping of zero-order wave and twin-image wave with real image wave during reconstruction, which degrades the reconstructed image quality and measurement results. In this letter, methodologies based on in-line digital holography have been explored and applied for dynamic measurements of MEMS. A lensless in-line digital holographic reflection microscope system is presented as the novel instrumentation for the dynamic characterization of MEMS. The developed methodology aims to use optical full-field dynamic measurement methods together with combined computational and experimental techniques, to implement comprehensive testability procedures in reliability testing of MEMS for dynamic applications.

In an in-line digital holographic configuration, the object and reference waves propagate along the same optical axis. The optical geometry of a reflection lensless digital holography microscopic system is shown in Fig. 1. A diverging laser beam from the fiber end provides the magnification in a lensless geometry. The beam is divided into two parts by using a beam splitter; one beam illuminates the sample and the other is incident on the plane mirror. The sample is illuminated by the diverging beam coming from the beam splitter. The scattered light from the sample (called object beam) is combined with the other diverging beam reflected from the mirror (called reference beam) and the resulting interference pattern is recorded by the CCD. The distance between the object and CCD controls the magnification of the system. Let (x, y) be the object plane and (ξ, η) be the hologram plane. The hologram, which is the interference

of the object wave $O(\xi,\eta)$ and reference wave $R(\xi,\eta)$, can be written as

$$\begin{aligned} H(\xi,\eta) = & |O(\xi,\eta)+R(\xi,\eta)|^2 \\ = & |O(\xi,\eta)|^2+|R(\xi,\eta)|^2+O^*(\xi,\eta)R(\xi,\eta) \\ & +O(\xi,\eta)R^*(\xi,\eta), \end{aligned} \tag{1}$$

where O^* and R^* are the complex conjugates of O and R, respectively.

The CCD, placed at the hologram plane, records the interference pattern as given in Eq. (1). For digital recording, the sampling theorem requires that the interference fringe spacing must be larger than the size of two pixels of CCD. The recorded pattern is converted into a two-dimensional (2D) array of discrete signals by using the sampling theorem. Let $M \times N$ be the total number of pixels of the CCD with corresponding sizes $\Delta\xi$ and $\Delta\eta$, and then the digitally sampled holograms $H(m,n)$ can be written as

$$\begin{aligned} H(m,n) = & [H(\xi,\eta)\otimes \mathrm{rect}(\frac{\xi}{\alpha\Delta\xi},\frac{\eta}{\beta\Delta\eta})] \\ & \times \mathrm{rect}(\frac{\xi}{M\Delta\xi},\frac{\eta}{N\Delta\eta})\mathrm{comb}(\frac{\xi}{\Delta\xi},\frac{\eta}{\Delta\eta}), \end{aligned} \tag{2}$$

where $\otimes$ represents the 2D convolution and $(\alpha,\beta)\in[0,1]$ are the fill factors of the CCD pixels.

The reconstruction of hologram is a diffraction process. The hologram $H(\xi,\eta)$ is illuminated by the reconstruction wave $R(\xi,\eta)$. The reconstructed wave field $U(x',y')$ at the image plane (x',y') at distance d' is given by the Fresnel diffraction equation[14]:

$$\begin{aligned} U(x',y') = & \frac{\mathrm{e}^{\mathrm{i}kd'}}{\mathrm{i}\lambda d'}\int_{-\infty}^{\infty}\int_{-\infty}^{\infty} H(\xi,\eta)R(\xi,\eta) \\ & \exp[\frac{\mathrm{i}\pi}{\lambda d'}\{(x'-\xi)^2+(y'-\eta)^2\}]\mathrm{d}\xi\mathrm{d}\eta. \end{aligned} \tag{3}$$

If the hologram recorded with CCD contains $M \times N$ pixels with pixel sizes $\Delta\xi$ and $\Delta\eta$ along the coordinates, respectively, and then the reconstructed field defined by

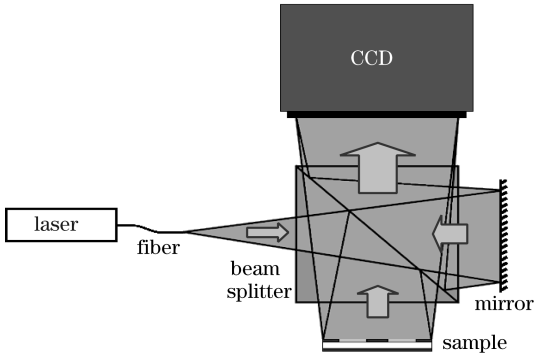

Fig. 1. Optical system for lensless DH in-line reflection microscope.

Eq. (3) converted to finite sums as [15]

$$\begin{aligned} U(k,l) = & \frac{\mathrm{e}^{\mathrm{i}kd'}}{\mathrm{i}\lambda d'}\mathrm{e}^{\mathrm{i}\pi\lambda d'(\frac{m^2}{M^2\Delta\xi^2}+\frac{n^2}{N^2\Delta\eta^2})} \\ & \times\sum_{k=0}^{M-1}\sum_{l=0}^{N-1} H(m,n)R(m,n) \\ & \mathrm{e}^{[\frac{\mathrm{i}\pi}{\lambda d'}(m^2\Delta\xi^2+n^2\Delta\eta^2)]}\mathrm{e}^{[-2\pi\mathrm{i}(\frac{mk}{M}+\frac{nl}{N})]}, \end{aligned} \tag{4}$$

where $k = 0,1,\cdots,$M-1; l=0,1,2,$\cdots, N-1$. Equation (4) is the discrete Fresnel transformation. The matrix $U(k,l)$ is the discrete Fourier transform of the product of $H(m,n)$, $R(m,n)$, and $\exp\{(\mathrm{i}\pi/\lambda d')(m^2\Delta\xi^2+n^2\Delta\eta^2)\}$. Thus the calculation of reconstructed wave field can be done effectively by using the fast Fourier transform (FFT) algorithm.

The numerically reconstructed wave field, because of in-line geometry, represents the real-image wave, twin-image wave, and zero-order term along the optical axis and can be written as

$$\begin{aligned} U(k,l) = & U_{\mathrm{real-image-wave}}(k,l) \\ & +U_{\mathrm{twin-image-wave}}(k,l) \\ & +U_{\mathrm{zero-order-wave}}(k,l). \end{aligned} \tag{5}$$

The pixel size of the numerically reconstructed real image varies with the reconstruction distance and is given by[15]

$$\Delta x' = \frac{\lambda d'}{M\Delta\xi}, \quad \Delta y' = \frac{\lambda d'}{N\Delta\eta}. \tag{6}$$

The image intensity I and phase ϕ at the real image plane can be calculated as

$$I = |U(k,l)|^2, \phi = \arctan[\mathrm{Im}(U(k,l))/\mathrm{Re}(U(k,l))]. \tag{7}$$

But, due to simultaneous presence of twin-image wave and zero-order term, the intensity and phase of the real image cannot be used directly for imaging and/or measurement applications.

In DH interferometry for dynamic measurement, both the amplitude and the phase difference of the two holograms recorded at two different states provide characteristics of dynamic phenomenon. The instantaneous dynamic deformation of any object can be measured using high speed CCD camera, digital holograms are recorded corresponding to the different deformations of the objects and their subtraction provides the dynamic changes. When an object placed at the plane (x,y) is illuminated by the coherent beam, the light wave reflected, scattered, or diffracted from the object surface can be written as

$$O(x,y) = O_0(x,y)\mathrm{e}^{\mathrm{i}\phi_0(x,y)}, \tag{8}$$

where $O_0(x,y)$ is the complex amplitude of the light and $\phi_0(x,y)$ is the phase representing the object surface properties. This object wave interferes with the in-line reference wave and a hologram is recorded using CCD. For different deformations of the object, the amplitude of the object wave is the same; however, the phase changes corresponding to the deformation. In-line holograms are recorded corresponding to different deformation states of

the object.

During reconstruction, the zero-order wave and the twin image overlap with this real image wave. Apart from a magnification term, the reconstructed wave can be written as

$$U(x',y') = O_0(x',y')\mathrm{e}^{\mathrm{i}\phi(x',y')} + U_{\mathrm{I+II}}, \tag{9}$$

where the first part of the right hand side is the reconstructed real image wave, and $U_{\mathrm{I+II}}$ is the sum of background reference wave (zero-order wave) and twin image wave. The background noise in the final reconstructed real image of the object is due to the zero-order wave and out-of-focus twin image wave and does not change with different deformation states of the same object. This is because the twin image forms on the opposite side of hologram plane relative to the real image and appears as a defocused image at the real image plane. In the case of small objects, the twin image wave diverges significantly at the real image plane. Also, when the hologram is reconstructed with a converging beam, the divergence of the out-of-focus twin image at the real image plane further increases, and thus the effect of phase becomes significantly negligible compared with the real image wave. Thus, in order to eliminate the background reference beam and the twin image, phases of the reconstructed image wave are calculated corresponding to the two different deformation states of the object and then subtracted. The numerically subtracted phase becomes the modulo 2π interference phase, which provides the deformation map. If $\phi_0(x,y)$ is the phase corresponding to the static state of the object (reference state) and $\phi_1(x,y)$ is the phase corresponding to the deformation state, and then the subtraction of the phases of numerically reconstructed in-line holograms can be written as

$$\Delta\phi_{2\pi} = \phi_1 - \phi_0. \tag{10}$$

For a sinusoidally vibrating object in the (x,y) plane, the instantaneous object wave $O'(x,y,t)$ at any instant scattered from the vibrating object is

$$O'(x,y,t) = O_0(x,y)\mathrm{e}^{\mathrm{i}\phi_0(x,y)}\mathrm{e}^{\mathrm{i}[\vec{K}\cdot\vec{z}_v(x,y,t)]}, \tag{11}$$

where $\phi_0(x,y)$ is the phase representing the mean deformation state of the vibrating object, $\vec{K}$ is the sensitivity vector, and $\vec{z}_v(x,y)$ is the amplitude of vibration.

For time-averaged recording, the frame capture time τ of the CCD should be larger than the period of object vibration[16]. The time-averaged object wave thus becomes

$$\begin{aligned} O(x,y) &= \frac{1}{\tau}\int_0^{\tau} O'(x,y,t)\mathrm{d}\tau \\ &= O_0(x,y)\exp\{\mathrm{i}\phi(x,y)\} \times J_0\{\vec{K}\cdot\vec{z}_v(x,y)\}, \end{aligned} \tag{12}$$

where J_0 is the zero-order Bessel function and $\phi(x,y)$ represents the phase of the object wave which contains the information both about mean static deformation and zeros of Bessel function, defined as

$$\phi(x,y) = \phi_o(x,y) + \phi_J(x,y), \tag{13}$$

where $\phi_0(x,y)$ contains object surface information and $\phi_J(x,y)$ is the time-averaged phase. The in-line reference wave interferes with the object wave from the vibrating object and thus the time-averaged hologram is recorded by the CCD.

The reconstructed wave, in this case, can be written as

$$U(x',y') = O_0(x',y')\mathrm{e}^{\mathrm{i}\phi(x',y')}J_0[\vec{K}\cdot\vec{z}(x',y')] + U_{\mathrm{I+II}}, \tag{14}$$

where the first term on the right hand side is the reconstructed real image wave and $U_{\mathrm{I+II}}$ is the background noise. This background noise in the final reconstructed real image of the object is due to the zero-order wave and out-of-focus twin image wave, and does not change significantly with different deformation states of the same object. However, since the speckle pattern changes stochastically between exposures, the background noise may not be exactly equal.

The amplitude and phase of the numerically reconstructed real image wave are, apart from a magnification term, as follows:

$$\begin{aligned} A(x',y') &= |U(x',y')| = O_0(x',y') \\ &\quad J_0\{\vec{K}\cdot\vec{z}_v(x',y')\}, \end{aligned} \tag{15}$$

$$\begin{aligned} \phi(x',y') &= \arctan\frac{\mathrm{Im}(U(x',y'))}{\mathrm{Re}(U(x',y'))} \\ &= \phi_o(x',y') + \phi_J(x',y'). \end{aligned} \tag{16}$$

In order to suppress the background noise, two time-averaged in-line holograms of the object are recorded. One corresponding to the reference state (either static or vibration) and the other is the vibration state. Consider an object vibrating at two different amplitudes $\vec{z}_1$ and $\vec{z}_2$ corresponding to the two states. The phases of the mean deformation states are ϕ_1 and ϕ_2, respectively. On numerical reconstruction, the wave fields can be written as

$$\begin{aligned} U_1(x',y') = {} & O_0(x',y')\mathrm{e}^{\mathrm{i}\phi_1(x',y')} \\ & J_0[\vec{K}\cdot\vec{z}_1(x',y')] + (U_{\mathrm{I+II}})_1 \end{aligned} \tag{17a}$$

for the refernce state, and

$$\begin{aligned} U_2(x',y') = {} & O_0(x',y')\mathrm{e}^{\mathrm{i}\phi_2(x',y')} \\ & J_0[\vec{K}\cdot\vec{z}_2(x',y')] + (U_{\mathrm{I+II}})_2 \end{aligned} \tag{17b}$$

for the vibration state, respectively. $(U_{\mathrm{I+II}})_1$ and $(U_{\mathrm{I+II}})_2$ do not change for different deformation states of the same object. Thus the subtraction of wave field provides the information about vibration behaviour of the objects free from background noise. To do this, the amplitude and phase of the individual wavefields are extracted first. The difference in amplitudes then provides the Bessel type vibration fringes while the difference of phase gives the mean deformation.

Experimental results are presented for dynamic interferometric measurements and vibration analysis. In dynamic interferometric measurements, a sequence of holograms is recorded during the dynamic changes in the sample and phase subtraction, between two different states, providing the dynamic deformation information of the sample. The experimental setup shown in Fig. 1 is used for thermal deformation study of the elements of a microheater device. A single mode fiber with a core diameter of 10 μm is attached to a He-Ne laser. The hologram is recorded using the CCD, having 960 $\times$

1280 pixels with 4.65×4.65 (μm) in size.

The microheater is fabricated through PolyMUMPs[17], a commercial three-layer polysilicon surface micromachining process used for MEMS applications. The optical microscopic image of the microheater sample is shown in Fig. 2. The active area of the microheater is fixed at 140×140 μm^2. The length, width, and spacing are varied to achieve different resistance values ranging from 420 to 1850 Ω. The sheet resistances of Poly-1 and Poly-2 are 10/square and 20/square, respectively. The temperature of microheater elements varies linearly with the input electrical power. However, larger temperatures lead to increased thermal stresses on the heater structures, resulting in mechanical deformation of the device. The dynamic deformations arising in the structure are analyzed using the presented system as a non-contact and non-destructive tool.

The electrodes are connected to the power supply. A series of holograms were recorded corresponding to the different voltages between the electrodes. Two points on different elements on the micro-heater are shown in Fig. 2. In order to measure the thermal deformation in micro-elements, the holograms are recorded by varying voltages from 1 to 10 V. The numerical reconstruction of the holograms is performed at different voltages and the phase information is reconstructed corresponding to each state. The subtraction of the phases of the deformed state (corresponding to the applied voltage) and reference state (without applying voltage) provides the deformation fringes. Figures 3(a)–(f) show the deformation fringes for the voltages of 1.0, 2.0, 3.0, 6.0, 7.0, and 8.0 V. Deformation fringes can be clearly observed, showing the different deformation value in electrodes. As expected, the number of fringes increases with the increase of voltage, which shows the increase in the thermal deformation corresponding to the applied voltages. It can be clearly observed that the deformation fringes are also expended in the other electrodes, particularly at larger voltages, which results in higher temperatures. Thus, this kind of analysis is particularly useful for full-field dynamic study of micro-size devices, where different components of the device showing different deformations subject to the same input conditions.

Vibration analysis of the aluminium nitride (AlN) cantilevers is performed using the time-averaged lensless in-line digital holographic microscopy system. AlN films have piezoelectric properties, and represent an alternative to piezoelectric transducer (PZT) films[18]. AlN

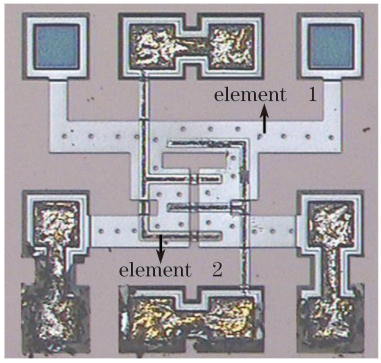

Fig. 2. MEMS micro-heater sample.

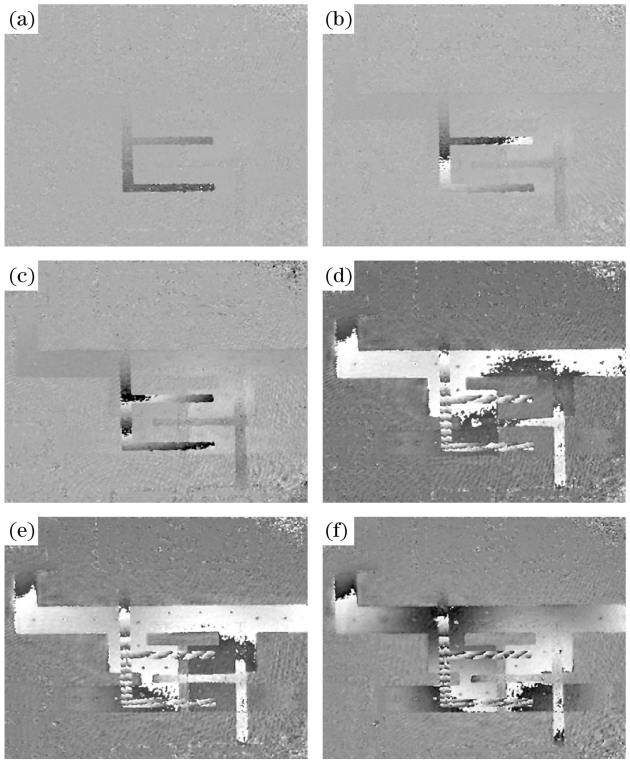

Fig. 3. Out-of-plane thermal deformation fringes in micro-elements as a function of applied voltages. (a) 1.0 V, (b) 2.0 V, (c) 3.0 V, (d) 6.0 V, (e) 7.0 V, and (f) 8.0 V.

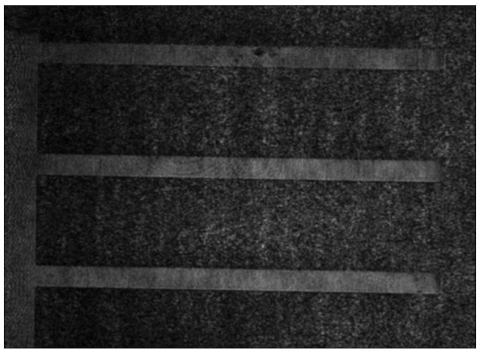

Fig. 4. Numerically reconstructed image of cantilevers.

cantilevers of size 800×50 μm are fabricated using surface micromachining process. The numerically reconstructed image of the three static cantilevers electronically connected together is shown in Fig. 4 and the vibration analysis of these cantilevers is presented here. The mode shapes of the vibrating cantilevers are obtained from the reconstruction of time-averaged in-line holograms. The amplitude of the reconstructed real image wave, which is modulated by the J_0 function, gives the mode pattern. The system shown in Fig. 1 is used for vibration analysis.

Time-averaged holograms are recorded corresponding to the resonant frequencies of the cantilevers. The mode shapes corresponding to the first, second, and third resonant frequencies are shown in Fig. 5, which is obtained by amplitude reconstruction of time-averaged holograms. The vibration modes shown are presented corresponding

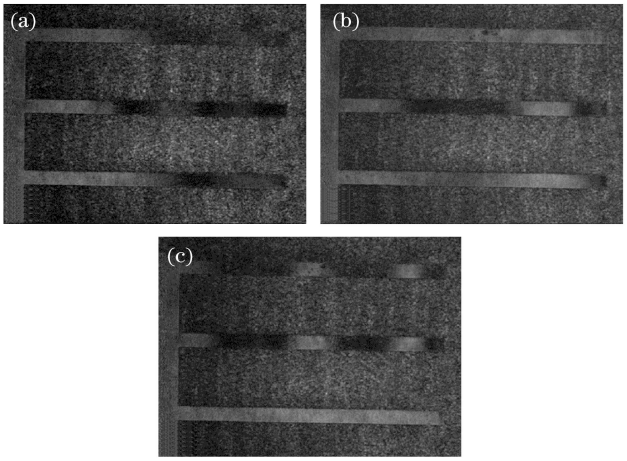

Fig. 5. Mode shapes corresponding to the resonant frequencies of (a) 30.46 kHz, (b) 191.40 kHz, and (c) 533.0 kHz.

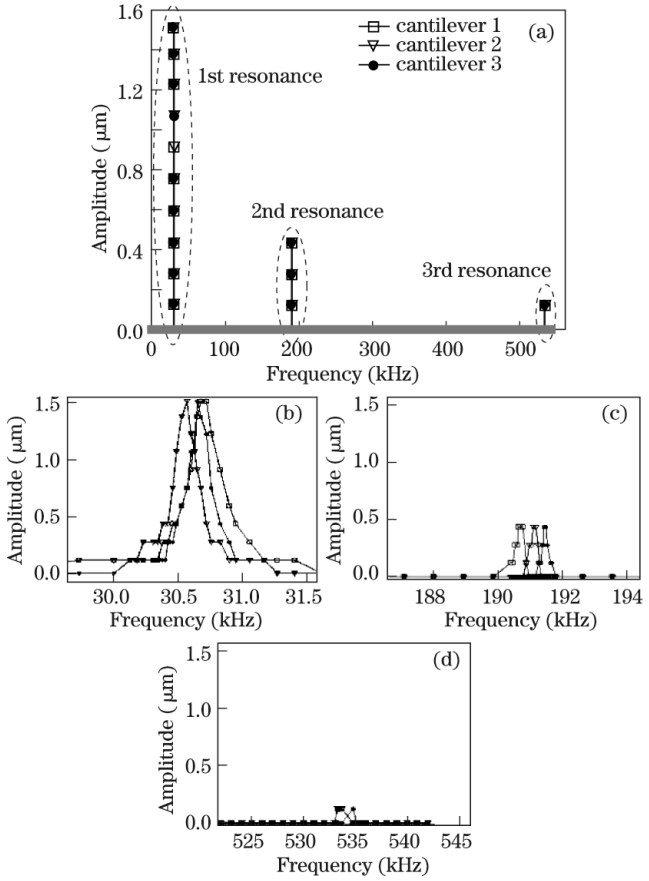

Fig. 6. (a) Frequency spectrum of the cantilevers, and resonant frequencies of cantilevers corresponding to (b) the first, (c) the second, and (d) the third resonant frequency.

to the first, second, and third frequencies at 30.46, 191.40, and 533.0 kHz, respectively.

The scanning frequencies corresponding to the resonant frequencies are performed and the amplitudes of the cantilevers are calculated. Equation (15) is used for vibration amplitude measurements. The factor $\vec{K} \cdot \vec{z}_v(x', y') = K z_v g'$, where $K = 2\pi/\lambda$, for the experiment system $\lambda = 0.6328$ μm and geometric factor $g' = 2$. This factor represents the zeros of zero-order

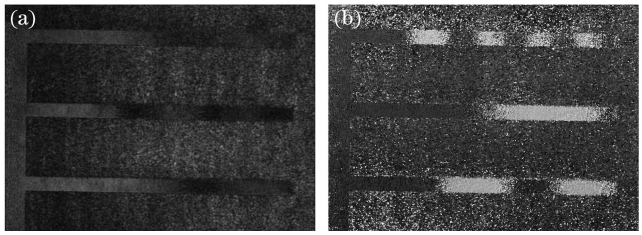

Fig. 7. (a) Time-averaged amplitude; (b) time-averaged phase.

Bessel function of the reconstructed image. The zeros of first order Bessel function used correspond to the dark fringes for calculating the amplitude values. The frequency spectrum of the cantilevers is shown in Fig. 6(a). As it can be clearly seen (Fig. 5) that all the cantilevers are not vibrating at the same resonant frequency; this is further explored in Figs. 6(b)–(d). Figure 6(b) shows the resonant frequency of each cantilever corresponding to the first resonant frequency, and similarly Figs. 6(c) and (d) show the second and third resonant frequencies, respectively.

The main advantage in using digital holography is to obtain the quantitative phase information of the reconstructed image wave. The numerically reconstructed phase from time-averaged holograms contains two parts, one (varying from $-\pi$ to $+\pi$) represents the object mean static state and the second part (binary values 0 and $\pm\pi$) is called time-averaged phase which shows the zeros of the J_0 function[19]. The amplitude reconstruction from time-averaged hologram is modulated by zero-order Bessel function, and thus the contrast of higher order fringes becomes quite poor because of the reduction in the intensity of Bessel function (Fig. 5). The better visibility of the vibration modes is possible to obtain using the time-averaged phase information. For pure sinusoidal vibration of the object, the subtraction of phases of time average from the reference hologram provides only the time-averaged phase. It is presented in Fig. 7. Figure 7(a) shows the amplitude reconstruction from the time-averaged hologram recorded for the first resonant frequency. It can be clearly seen that the contrast of higher order fringes is significantly poor, particularly in the case of the first (on the top) cantilever. Figure 7(b) shows the subtraction of phase of the time-averaged hologram from the reference state (static state), the time-averaged phase represents the binary jumps and thus the contrast of the fringes is significantly improved.

In conclusion, a lensless in-line digital holographic microscopy is presented as a novel tool for dynamic metrology for MEMS. The novelty is the incorporation of lensless magnification with in-line digital holography method to provide the compact geometry precisely suitable to fulfil the metrological requirements of micro-size objects. The methodologies of dynamic measurements are presented that simultaneous suppress the zero-order and twin image waves from the real image wave. Thermal deformation in micro-elements is presented as the first application of dynamic interferometry. The results are presented for full field analysis of a microheater device. The second application is presented for vibration characterization of cantilevers. Frequency shift is found in

the resonance frequencies of similar cantilevers. The presented system is thus a simple, compact, and powerful tool for MEMS and micro-systems inspection and characterization.

This work was financially supported by the National Research Foundation of Singapore under Proof of Concept (POC) scheme (No. 2008 NRF-POC0001-068).

References

1. C. M. Vest, *Holographic Interferometry* (Wiely, New York, 1992).
2. U. Schnars and W. Jüptner, Appl. Opt. **33,** 179 (1994).
3. L. Ma, H. Wang, Y. Li, and H. Jin, J. Opt. A: Pure Appl. Opt. **6,** 396 (2004).
4. A. Asundi and V. R. Singh, Meas. Sci. Technol. **17,** 75 (2006).
5. A. Asundi and V. R. Singh, Opt. Lett. **31,** 2420 (2006).
6. N. Maluf, *An Introduction to Microelectromechanical Systems* (Artech House, Boston, 2000).
7. M. J. Madou, *Fundamentals of Microfabrication* (CRC-Press, Boca Raton, 1998).
8. A. Asundi and V. R. Singh, J. Holography Speckle **3,** 103 (2006).
9. L. Xu, X. Peng, J. Miao, and A. Asundi, Appl. Opt. **40,** 5046 (2001).
10. G. Coppola, P. Ferraro, M. Iodice, S. De Nicola, A. Finizio, and S. Grilli, Meas. Sci. Technol. **15,** 529 (2004).
11. V. R. Singh, J. Miao, Z. Wang, G. Hegde, and A. Asundi, Opt. Commun. **280,** 285 (2007).
12. L. Xu, J. Miao, and A. Asundi, Opt. Eng. **39,** 3214 (2000).
13. L. Xu, P. Z. Guo, M. Jianmin, and A. Asundi, Opt. Express **13,** 2444 (2005).
14. J. W. Goodman, *Introduction to Fourier Optics* (McGraw-Hill, New York, 1996).
15. U. Schnars and W. P. O. Jüptner, Meas. Sci. Technol. **13,** R85 (2002).
16. R. L. Powell and K. A. Stetson, J. Opt. Soc. Am. **55,** 1593 (1965).
17. B. Jayaraman, N. Bhat, and R. Pratap, J. Micromech. Microeng. **19,** 085006 (2009).
18. A. Andrei, K. Krupa, M. Jozwik, P. Delobelle, L. Hirsinger, C. Gorecki, L. Nieradko, and C. Meunier, Sens. Actuat. A **141,** 565 (2008).
19. P. Picart, J. Leval, D. Mounier, and S. Gougeon, Appl. Opt. **44,** 337 (2005).